ACCSCIENCE PUBLISHING

International Journal of Bioprinting

RESEARCH ARTICLE

Printed cisplatin on microneedle arrays for transdermal delivery enhances olaparib-induced synthetic lethality in a mouse model of homologous recombination deficiency

Zoi Kanaki[1], Alexandra Smina[1], Chrysoula Chandrinou[2], Fotini E. Koukouzeli[1], Yiannis Ntounias[1], Nikolaos Paschalidis[1], Ilias Cheliotis[2], Marina Makrygianni[2], Jill Ziesmer[3], Georgios A. Sotiriou[3], Ioanna Zergioti[2], Constantin Tamvakopoulos[1], and Apostolos Klinakis[1]*

[1]Biomedical Research Foundation Academy of Athens, 4 Soranou Efessiou Street, 11527 Athens, Greece

[2]Department of Physics, School of Mathematical and Physical Sciences, National Technical University of Athens, Heroon Polytehneiou 9, 15780 Athens, Greece

[3]Department of Microbiology, Tumor and Cell Biology, Karolinska Institutet, SE-171 77 Stockholm, Sweden

(This article belongs to the *Special Issue: Laser bioprinting technologies*)

Abstract

Small molecule inhibitors targeting specific proteins are claiming a continuously growing share in cancer therapy, more commonly in combination with traditional chemotherapeutic drugs. While these inhibitors are taken orally, the majority of chemotherapies are administered through intravenous injection in the hospital premises. Alternative routes for chemotherapy administration would allow more frequent administration at lower dosing by the patient oneself, allowing combination treatment with reduced side effects. Here, we employed laser printing to prepare microneedles for transdermal delivery of cisplatin. Combination treatment with cisplatin transdermally and the poly (ADP-ribose) polymerase (PARP) inhibitor olaparib orally leads to effective treatment in a cancer xenograft mouse model *in vivo*, while reducing the risk for systemic side effects. This work opens new avenues in anti-cancer therapy by allowing the administration of chemotherapy without the need for intravenous injection alone or in combination with other therapies.

Keywords: Laser-induced forward transfer; Microneedles; Metronomic chemotherapy; Transdermal dosing; Synthetic lethality; Homologous recombination deficiency

***Corresponding author:**
Apostolos Klinakis
(aklinakis@bioacademy.gr)

Citation: Kanaki Z, Smina A, Chandrinou C, *et al*., 2023, Printed cisplatin on microneedle arrays for transdermal delivery enhances olaparib-induced synthetic lethality in a mouse model of homologous recombination deficiency. *Int J Bioprint*, 9(6): 0048. https://doi.org/10.36922/ijb.0048

Received: February 10, 2023
Accepted: March 23, 2023
Published Online: June 23, 2023

1. Introduction

Chemotherapy has been the cornerstone of anti-cancer therapy for several decades now. More recently, advances in next-generation sequencing allowed the identification of several actionable mutations which can be exploited therapeutically toward personalized approaches in cancer treatment[1]. Novel targeted therapies such as small molecules and antibodies that emerged after the 2000s showed great promise and were approved for

clinical use[2]. Among those, small molecules targeting poly (ADP-ribose) polymerase (PARP1/2) became the first drug designed to exploit synthetic lethality, a genetic concept described in model organism almost a century ago[3]. PARP1/2 proteins play an important role in the repair of single-strand breaks of the DNA[4].

An initial observation that cells carrying inactivating mutations in the *BRCA1* or *BRCA2* genes cannot survive PARP inhibition[5,6] catalyzed efforts to therapeutically target PARP proteins in cancer. Because women with germline mutations in these genes are at risk of developing breast and ovarian cancer, the first of a series of approvals by the U.S. Food and Drug Administration (FDA) for PARP1/2 inhibitors (PARPi) came in 2014 for the small molecule olaparib[7] against ovarian cancer in patients carrying *BRCA1* and *BRCA2* mutations. These mutations disrupt a DNA repair pathway known as homologous recombination (HR) repair, which is used to repair double-strand breaks[8]. PARP inhibition leads to unrepaired single-strand breaks, which in turn produce double-strand breaks, which cannot be repaired by HR-deficient cells, such as those carrying inactivating mutations in *BRCA1* and *BRCA2*. Eventually, these cells accumulate intolerable levels of DNA damage and are driven to cell death.

Besides the development of multiple PARPi which are approved for several indications as monotherapy[9], multiple studies have focused on the combination of PARPi with chemotherapy or other targeted therapies[10,11]. As serious dose-limiting toxicities were observed, a new trial (clinicaltrials.gov identifier: NCT00782574) aimed to establish the maximum tolerable dose and to evaluate the pharmacokinetics and preliminary efficacy of olaparib in combination with cisplatin in patients with advanced solid tumors. This study indicated that systematic administration of olaparib orally (100 mg or 200 mg twice a day) in combination with a standard single dose of cisplatin (75 mg/m^2) in the beginning of each 21-day cycle was not tolerable[12]. Some of the observed toxicities have been previously described in olaparib clinical trials, while others are clearly associated with cisplatin. Intermittent administration of olaparib at a lower dose (50 mg twice a day), which is close to the minimum dose of 60 mg twice daily that achieves 90% PARP inhibition[13], together with a reduced dose of cisplatin (60 mg/m^2), improved tolerability[12] and showed improved objective response rate, in comparison to olaparib monotherapy in previous phase II clinical trials[14-16]. These findings imply that there is obviously room for dose optimization. One solution could be the administration of lower doses of cisplatin in more frequent intervals. However, metronomic dosing of this platinum-based drug would be practically limited, since cisplatin is administered intravenously while PARPi is taken orally. Thus, alternative administration routes for cisplatin would be beneficial.

Microneedles (MNs) have emerged as an alternative approach for transdermal drug delivery because they allow transdermal administration, reduced pain, and delivery of molecules of high molecular weight. Drug-coated MNs, which are suitable for both hydrophilic and hydrophobic drugs[17-19], are ideal for low-dose administration of chemotherapeutic drugs, such as cisplatin[20-22]. This approach would eliminate the need to visit the hospital for intravenous administration of the drug. However, limited drug quantity and drug material waste, as well as uniformity of coating, are major limitations of this approach.

Recently, three-dimensional (3D) printing technologies have emerged as a valuable tool in the biomedical field. These technologies allow for the layer-by-layer construction of 3D structures using a variety of materials. The 3D printing approaches can be utilized to coat MNs by transporting little microdroplets of the active pharmaceutical ingredient (API) solution onto the MNs, hence creating uniform layers. Inkjet printing has been successfully used for MN coating for transdermal delivery of anti-cancer drugs[23-25]; however, limitations with the deposition of highly viscous inks onto a given substrate are encountered, and nozzle clogging is observed[26,27]. Laser-induced forward transfer (LIFT)[28], on the other hand, offers superior resolution, nozzle-free, and viscosity-independent laser printing of organic and inorganic material. We have previously used the LIFT technology to coat MNs with the chemotherapeutic drug gemcitabine. Transdermal application of the MNs in animal models leads to drug release, achieving substantial plasma levels[29].

Here, we exploited LIFT to coat MNs for transdermal delivery of cisplatin in mice. Pharmacokinetic studies indicated that transdermal application of the MNs produced cisplatin plasma levels that were low but detectable particularly at the later time points of the study (24 h). We generated mouse xenograft models using HR-deficient non-small cell lung cancer cells, and, by exploiting synthetic lethality, we showed that transdermal delivery of cisplatin in combination with oral olaparib leads to effective treatment *in vivo*.

2. Materials and methods

2.1. Materials

Olaparib and cisplatin (powder, 99.70%) were purchased from MedChemExpress (Monmouth Junction, NJ, USA). Ketamine was purchased from Richter Pharma AG (Wels, Austria). Xylazine was purchased from Neocell Pharmaceuticals (Athens, Greece). The LC-MS grade solvents ammonium acetate, formic acid (FA),

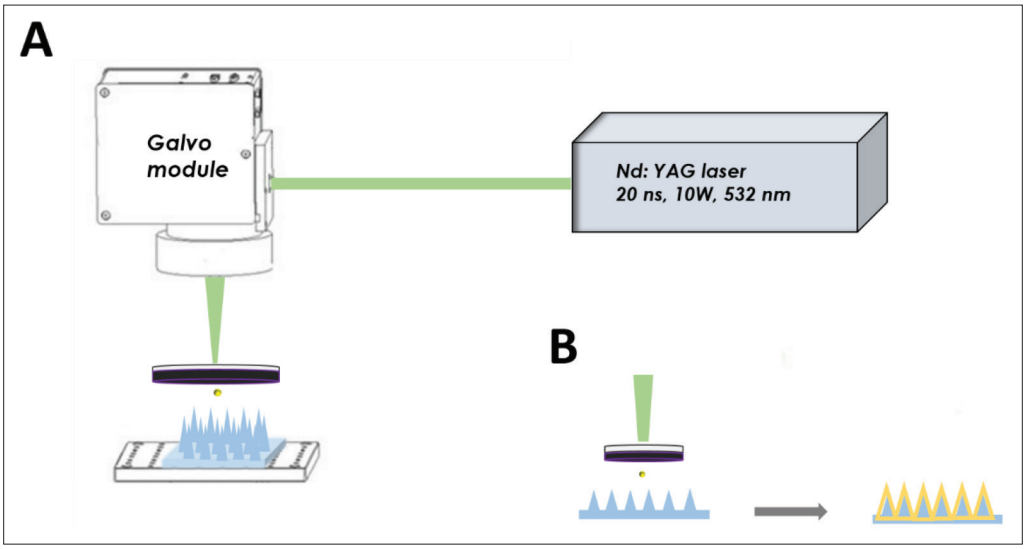

Figure 1. Schematic representation of the LIFT printing process for coating the MNs with cisplatin solution. (A) LIFT setup. (B) Coating process.

water (H_20), and methanol (≥99.8%) were procured from Fisher Scientific (Loughborough, UK). Acetonitrile (ACN; LC-MS grade) was bought from Carlo Erba (Milan, Italy). Sodium diethyldithiocarbamate trihydrate (DDTC) was obtained from Sigma Aldrich (Sigma-Aldrich Chemie GmbH, Munich, Germany). Blank (control) plasma was prepared via centrifugation of whole blood in a Heraeus Biofuge Pico. Midazolam was kindly provided by Onassis Cardiac Surgery Center (Athens, Greece) in the context of a research program in the form of a solution of Dormixal 15 mg/3 mL.

2.2. Cisplatin solubility

Due to the poor solubility properties of cisplatin in both H_20 and ethanol (EtOH)[30], solubility experiments were performed in distinct solvent mixtures to determine the optimal solvent system and highest concentration of the compound that would be compatible with the LIFT technology. We initially tested a range of cisplatin concentrations in H_20, achieving a soluble concentration of the compound (1 mg/mL). Following that, we checked cisplatin solubility in a solvent system of 10% glycerol in H_20, considering glycerol as a compatible reagent with the LIFT printing process. The solubility of cisplatin in the 10% glycerol in H_20 solvent system was low (<1 mg/mL). Since water mediates displacement of the chloride atoms in cisplatin (aquation) with unknown effects in the compound's pharmacological action, we further tested cisplatin solubility in saline and a 10% glycerol in saline solvent system, respectively. Since cisplatin was insoluble in the glycerol–saline mixture even at 1 mg/mL, saline was opted as the most ideal vehicle for the laser printing conditions and the *in vivo* administration.

2.3. MN array fabrication

Polymethylmethacrylate (PMMA; MW 120k, Sigma-Aldrich) was used to create MN arrays as previously reported[31] by dissolving it at 30 w/v% in ethyl lactate (≥98 %, Sigma-Aldrich) for 1.5 h at 150°C. The 100 pyramidal chambers in the MN molds (Micropoint Technologies) have a base length and height of 200 μm and 600 μm, respectively. The MN mold was cast with 50 mg of 30 w/v% PMMA, which was then centrifuged for 30 min at 3500 rpm and allowed to dry overnight in the fume hood.

2.4. LIFT process

The setup used for the LIFT printing of cisplatin solutions on MNs is designed for high-speed printing and is presented in Figure 1. The laser source is a DPSS Nd:YAG laser (Sol 10W 532 nm, BrightSolutions, Prado PV, Italy) emitting a wavelength of 532 nm with a maximum output power of 10 W. It delivers pulse duration of around 20 ns, with a repetition rate of 1–100 kHz, respectively, and a Gaussian beam profile. The laser beam is scanned with speeds up to 3 m/sec by utilizing a 2D galvanometric mirror scanning system (intelliSCAN III 10, SCANLAB, Puchheim, Germany) and an f-theta lens implementing a focal length of 100 mm. A beam expander configuration consisting of a two-lens setup transformed the output laser's beam into the desired 10-mm input size for the galvanometric scanning head. After leaving the laser source, the laser beam travels through the optical setup to determine its size and shape before irradiating a donor substrate that contains the substance to be deposited. The imaging system monitored the whole process in real time via a customized microscope system equipped with a camera enabling the accurate alignment of the target and substrate materials.

The donor substrate consisted of a transparent glass coated with a Ti film laser absorbing interlayer, onto which 5 μL of the cisplatin solution (1 mg/mL in saline) were drop cast. The receiver substrate was the MN patch onto which the cisplatin solution was transferred.

The printing process has been described previously[29]. Briefly, by focusing the laser beam onto the donor substrate, a high-pressure vapor pocket is produced at the interface of the deposited API solution and the Ti layer as a result of the donor's Ti layer absorbing the laser pulse. For each laser beam pulse, an nL droplet of cisplatin solution is printed onto the MN substrates as a result of this high-pressure vapor pocket expanding and propelling the supernatant fluid into a dynamic jet that drives the API solution to the receiver substrate at a high-impact velocity. The donor–receiver substrate distance was kept at 700 μm. On the MNs substrate, the laser transfer produced a continuous cisplatin film (5 × 5 mm) of 5 μL of the API solution. The LIFT process was repeated two more times on the same MN patch to achieve a total nominal amount of 15 μL of cisplatin solution. The coated MN patches' morphology was determined by scanning electron microscopy (SEM; FESEM Nova NanoSEM 230, by FEI Europe, Eindhoven, Netherlands).

2.5. Preparation of cisplatin stock and standard solutions

Stock solutions of cisplatin were prepared by dissolving approximately 3 mg of the compound in saline at a final concentration of 1 mg/mL. For preparation of cisplatin working solutions, serial dilutions in ACN:H_20 (1:1, v/v) were prepared in the concentration ranges of 50 ng/mL to 25 μg/mL. The internal standard midazolam was prepared by serially diluting Dormixal 15 mg/3 mL in ACN:H_20 (1:1, v/v) to 100 ng/mL. All stock and working solutions were stored at 4°C until the day of sample preparation in mouse plasma.

2.6. Pharmacokinetic studies

Cisplatin was administered in mice transdermally or intraperitoneally for evaluation of its pharmacokinetic properties per dosing route. For transdermal administration of cisplatin in mice, MN patches with 15 μg of LIFT-printed cisplatin were prepared. Furthermore, for intraperitoneal dosing of the platinum-based compound, a solution of 600 μg/mL in saline was prepared. Four mice were used for administration per dosing route, and all mice were equally dosed with 60 μg of cisplatin in MN or administered with cisplatin intraperitoneally. A serial cheek bleeding protocol was performed in mice at 2, 4, 24, and 72 h after MN application or intraperitoneal injection. The collected blood samples were placed in heparinized Eppendorf tubes, containing 10 μL heparin (5000 IU/mL), which were then placed immediately on ice and centrifuged for 10 min at 3000 rpm. Plasma was then stored in a -80°C freezer until the time of analysis. Mice were then euthanized.

For sample preparation, mouse plasma (50 μL) was placed in low-retention Eppendorf tubes and was spiked with 5 μL of cisplatin working solutions for the preparation of standards. A DDTC solution (1% DDTC in 0.1N NaOH) was then added (15 μL), and samples were vortexed and incubated in a water bath (40°C) for 30 min for the formation of the Pt-DDTC complex. Following the incubation step, 500 μL of cold ACN with internal standard (IS, midazolam, 1 ng/mL) was added to the precipitate of proteins. Subsequently, samples were vortexed for 2 min and centrifuged at 13,000 rpm for 10 min. The supernatant containing the Pt-DDTC complex and IS was transferred into glass tubes, and evaporation to dryness followed (50°C) for approximately 60 min. Samples were then reconstituted in 150 μL of H_20:ACN:FA (80:20:0.1%), centrifuged for 1 min, and then transferred into 96-well plates for liquid chromatography tandem mass spectrometry (LC-MS/MS) analysis[32].

2.7. Detection and quantification of cisplatin via LC-MS/MS

The amount of cisplatin in standard and unknown samples was determined via a LC-MS/MS methodology, previously reported by Agilent[32] with slight modifications, that quantifies cisplatin after derivatization with a DDTC reagent and formation of a Pt-DDTC complex. For the setup of the bioanalytical assay and sample analyses, a Triple Quad 5500+ LC-MS/MS System – QTRAP (AB SCIEX LLC, CA, USA) was used. Chromatographic separation of the analyte of interest was accomplished via a dC18 column (Waters, Atlantis, 2.1 × 50 mm, 3 μM) at a flow rate of 0.3 mL/min. Mobile phases included solution A (100% H_20, 0.1% formic acid [FA]), solution B (100% ACN), and needle wash (ACN:MeOH:H_20, 1:1:1), and injection volume for each sample was 10 μL. Elution of the analyte was achieved by applying a gradient system described as follows: T = 0–0.5 min for 95% A and 5% B, T = 1.0 min for 25% A and 75% B, T = 1.5 min for 10% A and 90% B, T = 2.5–4.0 min for 5% A and 95% B, T = 5.0 min for 95% A and 5% B. The transitions monitored via multiple reaction monitoring were m/z 492.5/422.1 for cisplatin at 2.67 min and m/z 326.1/291.1 at 2.44 min for midazolam, respectively. Additionally, transitions m/z 640.4/116.1 and 640.4/492.0 for cisplatin and 326.1/209.1 for midazolam, respectively, were used for confirmation of the bioanalytical result. The mass spectrometry (MS) system was operated using positive electrospray ionization mode (ESI). The applied bioanalytical methodology

and linearity of cisplatin was tested in a concentration range of 10–1000 ng/mL in mouse plasma with a limit of quantification (LOQ; at 10 ng/mL).

2.8. Cell expansion

H1437 cells were originally purchased from the American Type Culture Collection (ATCC). Cells were grown in Dulbecco's Modified Eagle's Medium (DMEM) supplemented with 10% fetal bovine serum and penicillin/streptomycin in a humidified chamber with 5% CO_2.

2.9. Efficacy study

NOD.Cg-Prkdc scid Il2rg tm1Wjl/SzJ mice (NSG mice; Stock No.: 005557)[33,34] were purchased from the Jax repository (Bar Harbor, ME, USA) and bred in individually ventilated cages under specific pathogen-free conditions, under veterinarian supervision, in full compliance with Federation of Laboratory Animal Science Associations recommendations in the Animal House Facility of the Biomedical Research Foundation of the Academy of Athens (BRFAA, Greece). All procedures for care and treatment of animals were approved by the Institutional Committee on Ethics of Animal Experiments and the Greek Ministry of Agriculture (Protocol #1392861, 28/12/22).

H1437 and H1437 KMT2C/KD cells were grown in DMEM supplemented with 10% fetal bovine serum and penicillin/streptomycin. Two million of cells were injected subcutaneously in the right flank of approximately 6-week-old male NSG mice. Tumor dimensions were measured with a caliper. When tumors grew to a diameter of approximately 0.3 cm, the mice were randomly assigned to groups. No exclusion criterion was applied. Four groups of at least 8 mice for either H1437 or the KMT2C/KD derivative were used for *in vivo* administration of olaparib, olaparib/cisplatin (Olap/C-IP), olaparib/cisplatin-MNs (Olap/C-MN), and vehicle. Cisplatin was administered to mice either transdermally or intraperitoneally. The efficacy of the vehicle cohort, Olap/C-IP cohort, and Olap/C-MN cohort was compared with one another. Cisplatin dosing was 3 mg/kg of cisplatin either intraperitoneally or transdermally, i.e., 60 μg/dose. Furthermore, 50 mg/kg olaparib in saline solution containing 12.5% dimethylsulfoxide (DMSO) and 12.5% Kolliphor® EL (Sigma-Aldrich) was administered orally on a daily basis. This is the typical amount of olaparib administered in mice for therapeutic purposes by most groups.

For transdermal application of cisplatin, mice were anesthetized with a ketamine:xylazine mix (90 mg/kg ketamine and 10 mg/kg xylazine) as previously described[29,35]. MN application onto the skin of mice was previously described[29]. Briefly, the opposite (left) non-tumor-bearing flank of the mouse was shaved, and four MN patches, with each containing 15 μg of cisplatin, were pressed with the thumb for approximately 2 min and then taped with 3M™ Steri-Strip™ Reinforced Adhesive Skin Closures (Digas, Athens, Greece) for 60 min. The vehicle cohort was treated daily with saline solution containing 12.5% DMSO and 12.5% Kolliphor® EL orally, and every 5 days with saline intraperitoneally. After 15 days, the mice were sacrificed with cervical dislocation, and the tumors were dissected, weighed, and photographed.

2.10. Cisplatin uptake measurement with mass cytometry-CyTOF

Frozen murine lung tumor tissue specimens were thawed in ice-cold dissociation solution (PBS supplemented with 2 mM EDTA). Tissues were further dissected into small pieces with an average size of approximately 27–30 mm^3 (3 × 3 × 3 mm). Then, using a culture dish filled with dissociation solution, tissue was pressed through a 100-μm nylon mesh with the plunger of a 5-mL syringe to prepare a cell suspension. During this step, the nylon mesh was in contact with the surface of the liquid in the culture dish. The mesh was then rinsed two or three times with ice-cold dissociation solution. Resulting suspension was then filtered through a 40-μm nylon mesh and adjusted on top of a 50-mL polypropylene Falcon tube, and dissociation solution was added to a final volume of 15 mL followed by centrifugation at 300 × *g* for 7 min. Cells were then washed twice with 5 mL of Maxpar Cell Staining Buffer (CSB) from Standard BioTools Inc. (SB; South San Francisco, CA, USA; formerly known as Fluidigm) and centrifuged at 300 × *g* for 5 min. Following washing, cells were fixed with freshly prepared 2%, filtered, methanol-free formaldehyde solution (prepared from 16% stock solution; Sigma-Aldrich) for 10 min at room temperature. Fixed cells were then centrifuged at 800 × *g* for 5 min and stained with DNA intercalator solution (1:1000 dilution of 125 μM Cell-ID™ Intercalator-Ir) in Maxpar Fix and Perm buffer (all from SB, USA) and incubated at 4°C overnight. The following day, cells were washed twice with CSB buffer and cell acquisition solution (SB, USA). Immediately before the acquisition, cells were re-suspended in cell acquisition solution supplemented with EQ Four Element Calibration Beads (EQ4 beads from SB), diluted 1:10, at a final cell concentration 1×10^6 cells/mL. Acquisition was performed on a Helios™ mass cytometry system (SB). To maximize data quality, the acquisition rate on the Helios was maintained at a rate of <400 events/s. Acquired data were normalized using EQ4 beads (SB method) with CyTOF software (version 10.7.1014). Normalized fcs files were analyzed with bivariate dot plots and histograms in FlowJo™ v10.8 Software (BD Life Sciences, Franklin Lakes, NJ, USA). Graphs and statistical analysis were performed using GraphPad Prism 9 (version 9.2.0 for Windows, GraphPad

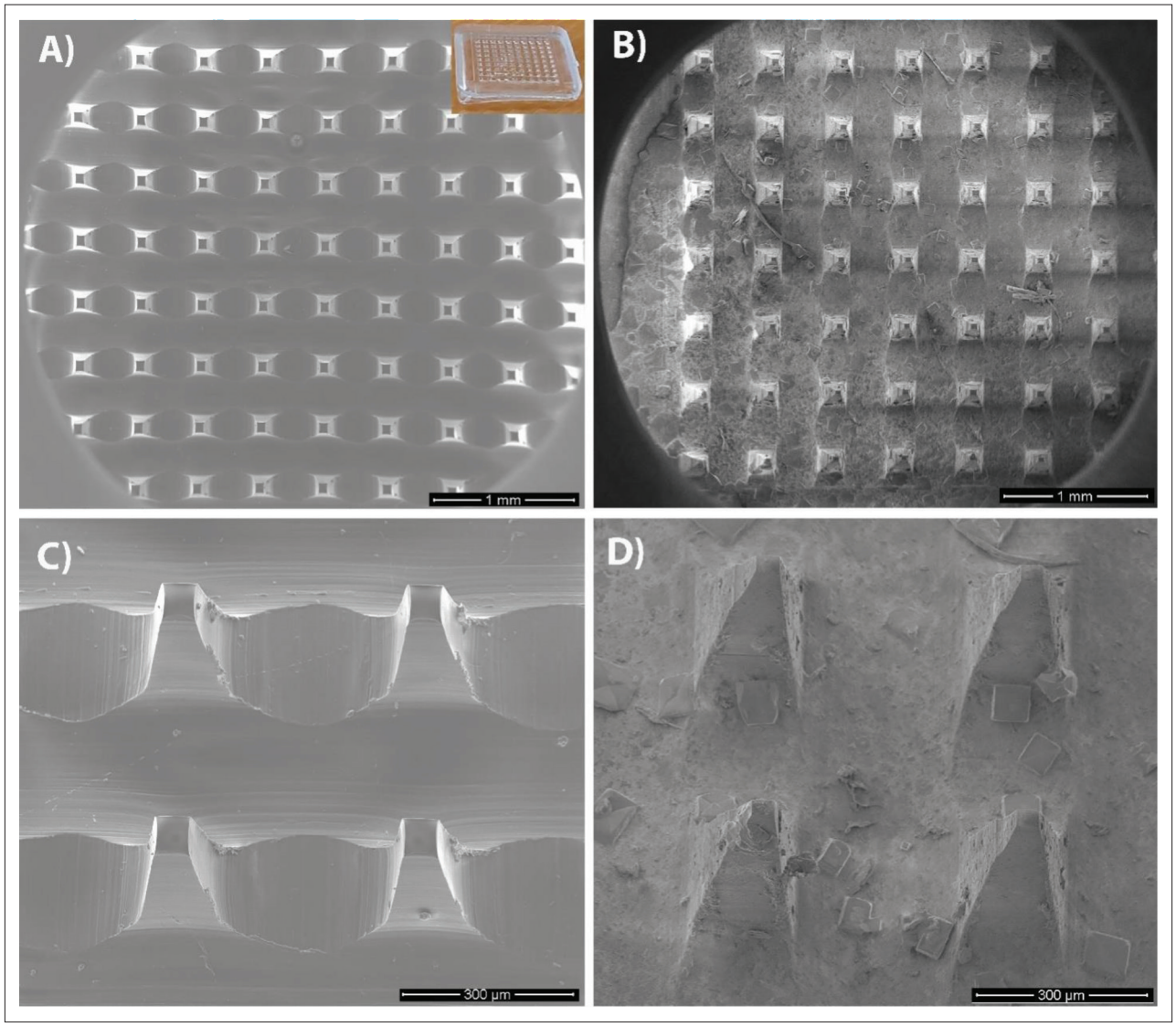

Figure 2. Representative SEM images before (A, C) and after (B, D) coating the MNs with cisplatin solution via the LIFT process. (A, B) Top view; (C, D) tilted at 20°. Insert in (A) shows the MN patch.

Software, San Diego, CA, USA). For comparisons, one-way analysis of variance (ANOVA) with Bonferroni correction was performed. Results were statistically significant at *adjusted $p < 0.05$ and ****adjusted $p < 0.0001$.

3. Results

3.1. Morphological characterization of LIFT-printed cisplatin solutions on MNs

The cisplatin solution was physically adsorbed onto the substrate as a result of the successful direct transfer of the API solution using LIFT printing, which depends on the high velocity and pressure that the liquid droplets have upon impact with the MNs substrate. The optimum printing fluence was 1 J/cm^2, while the laser spot size was 150 µm. Figure 2 shows SEM images from before and after coating the MNs with cisplatin via the LIFT process. It can be seen from the images that the cisplatin solution uniformly coated the MNs from the tip to the base and around the MN structures. The cubic structures present in the images are the salt crystals from the saline solution that was used for the API preparation[36].

3.2. Quantification of cisplatin in mouse plasma after intraperitoneal administration and administration with MNs

For the determination of cisplatin levels in mouse plasma after transdermal administration of the compound in MN, a LC-MS/MS method was developed and applied (depicted in Figure 3). Intraperitoneal injection of cisplatin was also

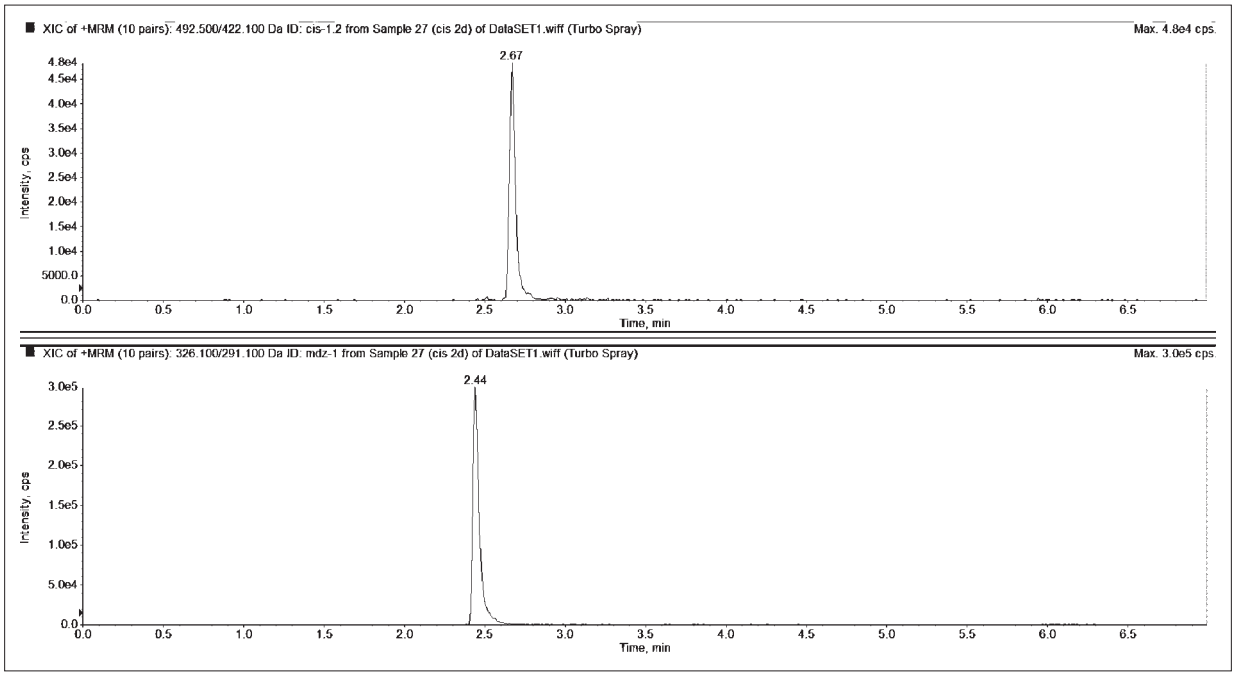

Figure 3. Representative LC-MS/MS chromatogram for cisplatin in mouse plasma at 4 h following intraperitoneal dosing of 60 μg in mice. For detection and quantification of cisplatin in plasma, the transition 492.5/422.1 with RT 2.67 min was used. Midazolam was used as internal standard (IS) with transition 326.1/291.1 and RT 2.44 min.

performed with the same dosing (60 μg for 20-g mice), in order to compare the levels of the compound in circulation between the distinct routes of administration. The 60 μg cisplatin corresponding to a 3 mg/Kgr dose is 50% of the standard dose that our group and others routinely use in mouse models of cancer for *in vivo* treatment.

Following intraperitoneal dosing of 60 μg of cisplatin in mice, plasma concentrations peaked at 2 and 4 h with average concentrations at 263 ± 63 ng/mL and 359 ± 28 ng/mL, respectively. At 3 days post dosing, average plasma concentrations decreased to approximately 10 ± 2 ng/mL. Previous findings from Johnsson *et al.*[37] reported concentrations of approximately 500 ng/mL in mouse whole blood and serum after a 3.75 mg/kg of cisplatin intraperitoneal dose in mice at 1 h post dosing. Administration of the same amount of cisplatin (60 μg) in mice via transdermal MN application yielded low concentrations of the compound at 2 and 4 h in plasma with concentrations of Below Limit of Quantification (BLQ; detected values were 5 and 6 ng/mL respectively). It is noteworthy, however, that although cisplatin levels declined 24 h post intraperitoneal administration, detectable amounts of the compound in plasma were found at 24 and 72 h after MN dosing, with concentrations of 21 ± 2.5 ng/mL and 9 ± 2 ng/mL, respectively. The results are depicted in Figure 4. The data provide some evidence for sustained release of cisplatin in bloodstream when loaded onto MN substrates. However, further experiments are required to confirm this observation.

3.3. Efficacy studies in mouse models of cancer

It has been previously shown that loss of the lysine (K)-specific methyltransferase 2C (KMT2C, also known as MLL3), which belongs to the mixed-lineage leukemia (MLL) family of histone methyltransferases, leads to HR deficiency in various cell types[38-40]. We have also shown that human cancer cell lines in which KMT2C levels have been knocked down with shRNAs present an exceptional response to the PARPi ilaparib[38]. *KMT2C* is mutated in 15% of human non-small cell lung cancer (TCGA PanCancer Atlas). On the other hand, HR deficiency and the potential use of PARPi in lung cancer are becoming fields of intense research in the field of cancer therapeutics. Mutation in genes encoding proteins involved in the HR repair or DNA damage response in general is identified in human lung cancer cases, while mutations signatures implying HR deficiency are also identified[41-43].

To assess whether the HR deficiency can be exploited therapeutically through combination therapy with olaparib orally and cisplatin through transdermal delivery of MNs printed with cisplatin, we used the non-small cell lung cancer cell line H1437, in which *KMT2C* has been knocked down with lentiviral expression of shRNAs[38]. When tumors grew to a diameter of approximately 0.3 cm, mice

A

Samples	Average Calculated Concentration of Cisplatin in Mouse Plasma ± SEM (ng/mL)
2h IP	263 ± 63
4h IP	359 ± 28
24h IP	157 ± 41
72h IP	10 ± 2
2h MN	BLQ (5)
4h MN	BLQ (6)
24h MN	21 ± 3
72h MN	9 ± 2

B

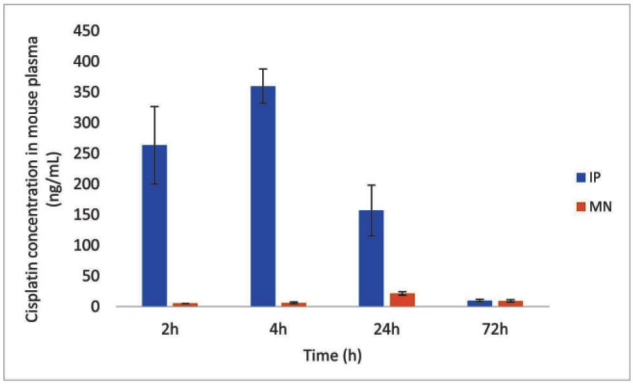

Figure 4. Determination of cisplatin levels in mouse plasma following intraperitoneal dosing and administration in MN. (A) Table presents the average of the quantified concentrations of cisplatin in mouse plasma at 2, 4, 24, and 72 h after administration in MN and intraperitoneal injection (n = 4). (B) Comparison of cisplatin concentrations in plasma after dosing with MN and intraperitoneal administration at 4 timepoints. Each timepoint was evaluated in quadruplicates for both dosing routes, and results are presented as average concentration ± standard error of the mean (SEM). Abbreviations: IP, intraperitoneal; MN, microneedle.

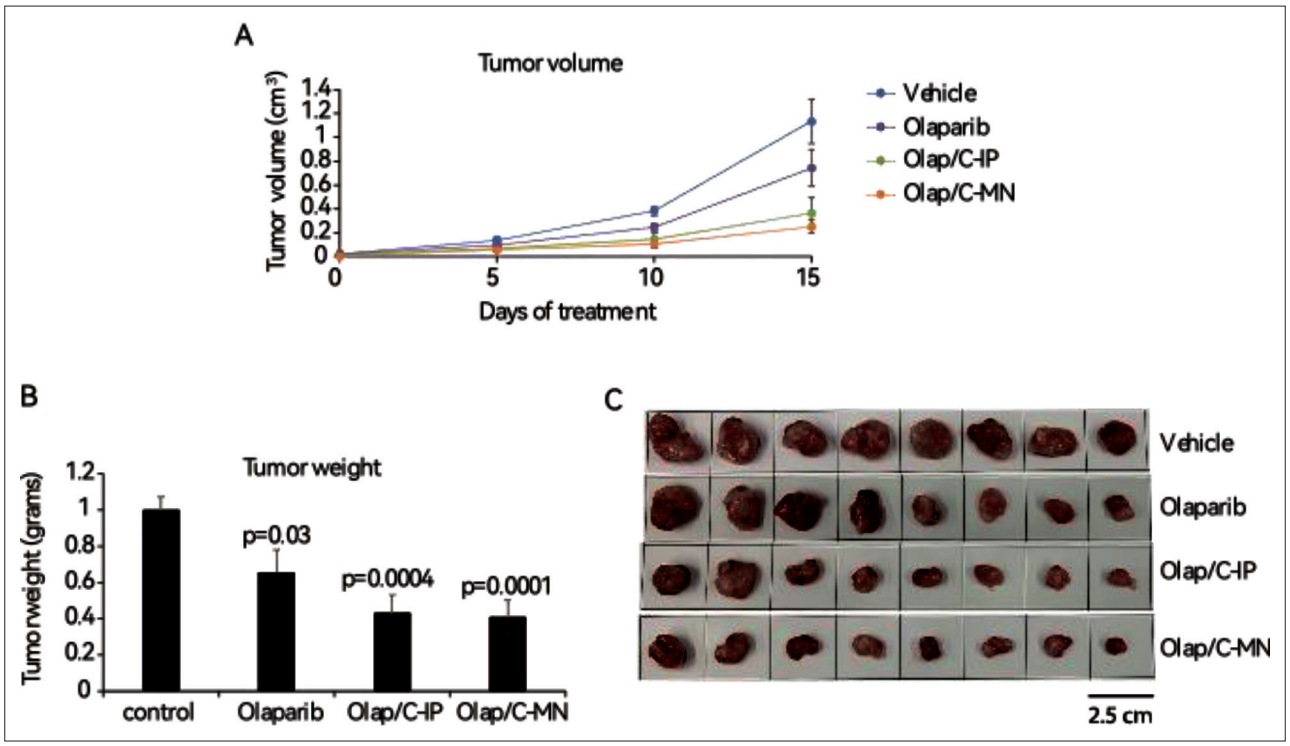

Figure 5. *In vivo* treatment of HR-deficient cells. (A) Plot indicating tumor volume during treatment. (B) Tumor weight at the end of the treatment. For (A) and (B), average of all tumors (n = 8) within indicated cohorts is shown. (C) Photograph of dissected tumors on the last day of treatment.

were allocated into four groups. While oral olaparib alone was effective in slowing down tumor growth, application of the transdermal MNs on days 0, 5, and 10 practically blocked tumor growth *in vivo*, as indicated by tumor volume (Figure 5A) and tumor weight (Figure 5B and C). These results showed that synthetic lethality is much higher when the combinatorial olaparib and cisplatin treatment is used.

This phenomenon is specific for the HR-deficient H1437 KMT2C/KD cells, as indicated by experiments with the parental cell line. As indicated in Figure 6, olaparib alone had a negligible effect, while combination with transdermal cisplatin, though more effective, had an effect that was less pronounced than that in the KMT2C/KD cells, further supporting the superior efficacy of PARPi in HR-deficient cells.

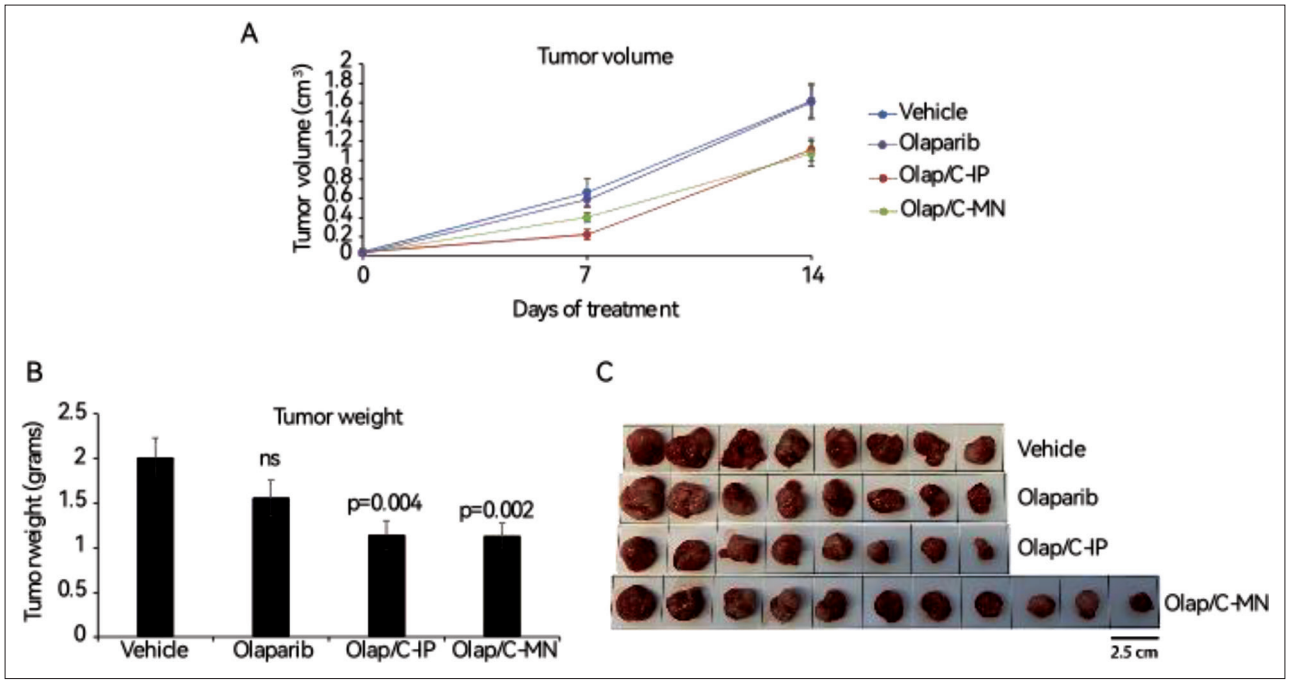

Figure 6. *In vivo* treatment of HR-proficient cells. (A) Plot indicating tumor volume during treatment. (B) Tumor weight at the end of the treatment. For (A) and (B), average of all tumors within indicated cohorts is shown. (C) Photograph of dissected tumors on the last day of treatment.

3.4. Cisplatin uptake

To measure cisplatin uptake at the single cell level, we employed mass cytometry-CyTOF (cytometry by time-of-flight) technology. In this technique, single cells are vaporized, atomized, and ionized allowing the atomic composition of each cell to be measured by a time-of-flight mass spectrometry system (ICP TOF MS)[44]. The presence of Pt, rather than intact cisplatin, in the cells is detected using this mass cytometry-CyTOF technology. As expected, intraperitoneal administration achieves higher Pt, derived from cisplatin amount in the tumors, both in terms of percentage of cells with detectable levels (99.2% vs. 64.7%), and mean intensity of positive cells (10 vs. 500) (Figure 7). The results are consistent with the findings from the pharmacokinetic study, in which cisplatin was monitored in plasma.

Our results indicate that olaparib treatment in HR-deficient tumors can be combined with the application of transdermal MNs for the administration of cisplatin at lower doses, avoiding the need for hospital trips, while ameliorating or even eliminating toxic side effects associated with the high intravenous dosing of cisplatin.

4. Discussion

Since the 2000s, an explosion in the development of new targeted therapies has revolutionized the field of cancer treatment. Targeted therapies are rarely administered alone. Instead, in the majority of schemes, these therapies are combined with chemotherapeutic drugs. Besides the opportunity for personalized treatment as a result of molecular indications and the generally less severe side effects, many targeted therapies offer the advantage of oral administration daily or even twice daily without the need for hospital visit. Chemotherapies, on the other hand, are mostly administered intravenously, requiring long stays at the hospital, often for a whole day. Moreover, patients receive a very high dose of the chemotherapeutic drug, leading to a high systemic concentration, which declines quickly until the new treatment. Thus, alternative methods for anti-cancer drug administration need to be developed. An interesting solution is oral metronomic dosing, which facilitates frequent drug administration by the patient[45]. We recently proposed transdermal MNs for metronomic dosing with gemcitabine[29].

API-coated MNs can be used for delivery of both hydrophilic and hydrophobic drugs[18,19]. Their ideal use is for low-dose administration of potent drugs, which are efficacious at low circulating amounts. There have been many methods employed in the past, such as dip coating[46], gas jet drying[47], and spray coating[48] with noted limitations[49,50], such as the difficult coating procedure because of the limited amount of drug coating, uniform coating, material waste, and precise drug dosing. In the last decade, 3D printing technologies such as inkjet printing, thermal, piezoelectric, and electrostatic printing, extrusion bioprinting, and LIFT have been used. As mentioned above, inkjet printing has been used before[25];

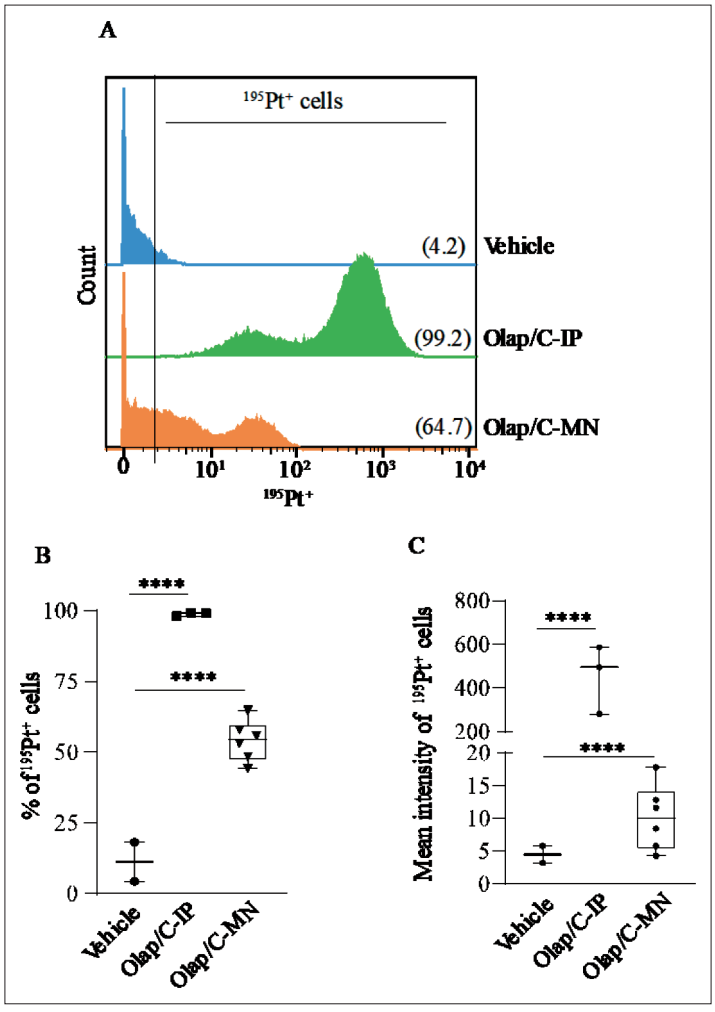

Figure 7. Analysis of cisplatin uptake in single cells from murine lung tumor tissue with mass cytometry-CyTOF. (A) shows the representative histogram displaying distribution of cisplatin (195Pt)-positive cells (% number in brackets) in lung tumor tissue of mice treated with vehicle, Olap/C-IP, or Olap/C-MN. Box and whiskers plots of % of 195Pt cells and mean intensity of 195Pt in all samples analyzed are shown in (B) and (C), respectively.

however, it has limitations with high-viscosity materials, due to the excessive force required to eject highly viscous drops. Moreover, inkjet printing is also associated with nozzle clogging[26,27]. It should also be noted that with most conventional drug coating approaches on MNs, the amount of API used on the MNs prior to coating is not controlled, but rather the eventual drug loading is only calculated using loading efficiency equations, after the coating is applied[51,52]. LIFT is highly efficient as it only utilizes the amount that is needed for each printing, thus reducing API and solvent waste. PARPi have emerged as promising therapy for tumors with HR deficiency leading to prolonged and sustained clinical response[53]. Though initially approved for ovarian and breast cancer patients carrying germline mutations in *BRCA1* and *BRCA2*, PARPi are now approved for pancreatic ductal adenocarcinoma[54] and prostate adenocarcinoma[55] with mutations in *BRCA1/2* and HR-related genes, respectively. In addition, additional PARPi were approved as maintenance, first-line, or second-line therapy in ovarian carcinoma, based on somatic *BRCA1/2* mutations, HR deficiency score (independently or in consideration of *BRCA1/2* mutations), or even without any HR deficiency-related indication if tumors responded favorably to cisplatin treatment. The rapidity of new approvals, revisions, and withdrawals of existing PARPi approvals indicates how dynamic this field is, with second-generation PARPi already under development. The general consensus in the field is that *BRCA1* and *BRCA2* mutations alone are not sufficient to stratify patients with solid malignancies who can benefit from PARPi. Mutations in other DNA repair genes, next-generation sequencing panels, and functional assays assessing HR repair are being employed in ongoing clinical studies[56]. Due to its frequency and dire prognosis, lung

cancer is attracting great interest in these studies. In this regard, tumors with mutations in *KMT2C*, which encodes a histone modifier with a rather indirect role in HR repair, emerge as a promising stratification marker for identifying patients who could benefit from PARPi. Together with identifying tumors with somatic mutations in HR-related genes and/or proven HR deficiency through molecular analysis or functional assays, this collection of diagnostic techniques can very likely identify patients who comprise a significant portion of the total lung cancer cases.

Since PARPi interfere with DNA damage repair, combination with other DNA-damaging agents such as cisplatin could be advantageous. Clinical practice, however, has indicated that combination of PARPi and cisplatin at the respective standard monotherapy dose is intolerable due to toxicity. Their combination, however, at lower dose seems to lead to clinical benefit in HR-deficient tumors[12]. Cisplatin intercalates into DNA generating intrastrand and interstrand adducts that, if not resolved, physically obstruct DNA polymerases during DNA replication, leading to the generation of double-strand breaks[57]. Cisplatin could remain in the human body, and traces of it can be found in the urine of patients even after 8 years from the treatment[58]. We thus hypothesize that because of its high potency and long excretion kinetics, even low levels of cisplatin could lead to increased DNA damage. Because PARPi is efficacious already as monotherapy in HR-deficient tumors, we hypothesize that even low levels of cisplatin are sufficient to sensitize cells to PARPi and maximize synthetic lethality.

To eliminate the need for hospital visit for intravenous administration of cisplatin, we have developed transdermal MNs which have been coated with cisplatin through LIFT technology. Cisplatin can be readily detectable in the blood stream and also in the tumors in mouse models of non-small cell lung cancer. Although these levels are lower than those achieved through intraperitoneal administration, the two approaches have comparable efficacy when combined with oral olaparib. The obvious advantage of transdermal administration of cisplatin without the need for hospital visits, as well as the ability to precisely adjust the dose with the use of LIFT technology, offers an attractive approach for combination therapies with cisplatin.

5. Conclusion

This work demonstrates for the first time that cisplatin printed onto MNs can be used for transdermal administration in mouse models of cancer. Transdermally-administered cisplatin reaches the bloodstream as well as the tumor itself, and although drug levels are lower than those obtained with intraperitoneal injection, they are sufficient to achieve strong response in HR-deficient lung tumors when the treatment is combined with oral administration of the olaparib. The proposed approach alleviates the cytotoxic side effects of the combination therapy while eliminating the need for intravenous administration of cisplatin in the hospital.

Acknowledgments

None.

Funding

This work has been co-financed by the European Union and Greek national funds through the Operational Program Competitiveness, Entrepreneurship, and Innovation, under the call RESEARCH–CREATE–INNOVATE (project code: T1EDK-00976). G.A.S. acknowledges funding from the European Research Council (ERC) under the European Union's Horizon 2020 research and innovation program (ERC Grant agreement no. 758705).

Conflict of interest

The authors declare no conflict of interest.

Author contributions

Conceptualization: Zoi Kanaki, Constantin Tamvakopoulos, Ioanna Zergioti, Apostolos Klinakis

Formal analysis: Zoi Kanaki, Alexandra Smina, Chrysoula Chandrinou, Ilias Cheliotis, Georgios A. Sotiriou, Apostolos Klinakis

Investigation: Zoi Kanaki, Chrysoula Chandrinou, Fotini E. Koukouzeli, Yiannis Ntounias, Nikolaos Paschalidis, Marina Makrygianni, Jill Ziesmer, Constantin Tamvakopoulos, Apostolos Klinakis

Methodology: Zoi Kanaki, Alexandra Smina, Chrysoula Chandrinou, Fotini E. Koukouzeli, Yiannis Ntounias, Nikolaos Paschalidis, Ilias Cheliotis, Jill Ziesmer, Georgios A. Sotiriou, Ioanna Zergioti, Constantin Tamvakopoulos, Apostolos Klinakis

Writing – original draft: Zoi Kanaki, Alexandra Smina, Chrysoula Chandrinou, Nikolaos Paschalidis, Jill Ziesmer, Georgios A. Sotiriou, Constantin Tamvakopoulos, Ioanna Zergioti, Apostolos Klinakis

Writing – review & editing: Zoi Kanaki, Alexandra Smina, Chrysoula Chandrinou, Nikolaos Paschalidis, Jill Ziesmer, Georgios A. Sotiriou, Constantin Tamvakopoulos, Ioanna Zergioti, Apostolos Klinakis

Ethics approval and consent to participate

All procedures for care and treatment of animals were approved by the Institutional Committee on Ethics of

Animal Experiments and the Greek Ministry of Agriculture (Protocol #1392861, 28/12/22).

Consent for publication

Not applicable.

Availability of data

Data available on request.

References

1. Tsimberidou AM, Fountzilas E, Nikanjam M, *et al.*, 2020, Review of precision cancer medicine: Evolution of the treatment paradigm. *Cancer Treat Rev*, 86(June): 102019.

   https://doi.org/10.1016/j.ctrv.2020.102019

2. Zhong L, Li Y, Xiong L, *et al.*, 2021, Small molecules in targeted cancer therapy: Advances, challenges, and future perspectives. *Signal Transduct Target Ther*, 6(1): 201.

   https://doi.org/10.1038/s41392-021-00572-w

3. Lord CJ, Ashworth A, 2017, PARP inhibitors: Synthetic lethality in the clinic. *Science*, 355(6330): 1152–1158.

   https://doi.org/10.1126/science.aam7344

4. Ray Chaudhuri A, Nussenzweig A, 2017, The multifaceted roles of PARP1 in DNA repair and chromatin remodelling. *Nat Rev Mol Cell Biol*, 18(10): 610–621.

   https://doi.org/10.1038/nrm.2017.53

5. Farmer H, McCabe N, Lord CJ, *et al.*, 2005, Targeting the DNA repair defect in BRCA mutant cells as a therapeutic strategy. *Nature*, 434(7035): 917–921.

   https://doi.org/10.1038/nature03445

6. Bryant HE, Schultz N, Thomas HD, *et al.*, 2005, Specific killing of BRCA2-deficient tumours with inhibitors of poly(ADP-ribose) polymerase. *Nature*, 434(7035): 913–917.

   https://doi.org/10.1038/nature03443

7. Menear KA, Adcock C, Boulter R, *et al.*, 2008, 4-[3-(4-cyclopropanecarbonylpiperazine-1-carbonyl)-4-fluorobenzyl]-2H-phthalazin-1-one: a novel bioavailable inhibitor of poly(ADP-ribose) polymerase-1. *J Med Chem*, 51(20): 6581–6591.

   https://doi.org/10.1021/jm8001263

8. Moynahan ME, Jasin M, 2010, Mitotic homologous recombination maintains genomic stability and suppresses tumorigenesis. *Nat Rev Mol Cell Biol*, 11(3): 196–207.

   https://doi.org/10.1038/nrm2851

9. Kim D, Nam HJ, 2022, PARP inhibitors: Clinical limitations and recent attempts to overcome them. *Int J Mol Sci*, 23(15).

   https://doi.org/10.3390/ijms23158412

10. Vikas P, Borcherding N, Chennamadhavuni A, *et al.*, 2020, Therapeutic potential of combining PARP inhibitor and immunotherapy in solid tumors. *Front Oncol*, 10(April): 570.

    https://doi.org/10.3389/fonc.2020.00570

11. Klinakis A, Karagiannis D, Rampias T, 2020, Targeting DNA repair in cancer: Current state and novel approaches. *Cell Mol Life Sci*, 77(4): 677–703.

    https://doi.org/10.1007/s00018-019-03299-8

12. Balmana J, Tung NM, Isakoff SJ, *et al.*, 2014, Phase I trial of olaparib in combination with cisplatin for the treatment of patients with advanced breast, ovarian and other solid tumors. *Ann Oncol*, 25(8): 1656–1663.

    https://doi.org/10.1093/annonc/mdu187

13. Fong PC, Boss DS, Yap TA, *et al.*, 2009, Inhibition of poly(ADP-ribose) polymerase in tumors from BRCA mutation carriers. *N Engl J Med*, 361(2): 123–134.

    https://doi.org/10.1056/NEJMoa0900212

14. Audeh MW, Carmichael J, Penson RT, *et al.*, 2010, Oral poly(ADP-ribose) polymerase inhibitor olaparib in patients with BRCA1 or BRCA2 mutations and recurrent ovarian cancer: A proof-of-concept trial. *Lancet*, 376(9737): 245–251.

    https://doi.org/10.1016/S0140-6736(10)60893-8

15. Tutt A, Robson M, Garber JE, *et al.*, 2010, Oral poly(ADP-ribose) polymerase inhibitor olaparib in patients with BRCA1 or BRCA2 mutations and advanced breast cancer: A proof-of-concept trial. *Lancet*, 376(9737): 235–244.

    https://doi.org/10.1016/S0140-6736(10)60892-6

16. Gelmon KA, Tischkowitz M, Mackay H, *et al.*, 2011, Olaparib in patients with recurrent high-grade serous or poorly differentiated ovarian carcinoma or triple-negative breast cancer: A phase 2, multicentre, open-label, non-randomised study. *Lancet Oncol*, 12(9): 852–861.

    https://doi.org/10.1016/S1470-2045(11)70214-5

17. Larraneta E, Lutton REM, Woolfson AD, *et al.*, 2016, Microneedle arrays as transdermal and intradermal drug delivery systems: Materials science, manufacture and commercial development. *Mat Sci Eng R*, 104(June): 1–32.

    https://doi.org/10.1016/j.mser.2016.03.001

18. Pearton M, Saller V, Coulman SA, *et al.*, 2012, Microneedle delivery of plasmid DNA to living human skin: Formulation coating, skin insertion and gene expression. *J Control Release*, 160(3): 561–569.

    https://doi.org/10.1016/j.jconrel.2012.04.005

19. Zhao X, Coulman SA, Hanna SJ, *et al.*, 2017, Formulation of hydrophobic peptides for skin delivery via coated microneedles. *J Control Release*, 265(November): 2–13.

    https://doi.org/10.1016/j.jconrel.2017.03.015

20. Lan X, Zhu W, Huang X, *et al.*, 2020, Microneedles loaded with anti-PD-1-cisplatin nanoparticles for synergistic cancer immuno-chemotherapy. *Nanoscale*, 12(36): 18885–18898.

    https://doi.org/10.1039/d0nr04213g

21. Lan X, She J, Lin DA, *et al.,* 2018, Microneedle-mediated delivery of lipid-coated cisplatin nanoparticles for efficient and safe cancer therapy. *ACS Appl Mater Interfaces*, 10(39): 33060–33069.

    https://doi.org/10.1021/acsami.8b12926

22. Fu JJ, Li CW, Liu Y, *et al.*, 2020, The microneedles carrying cisplatin and IR820 to perform synergistic chemo-photodynamic therapy against breast cancer. *J Nanobiotechnol,* 18(1): 146.

    https://doi.org/10.1186/s12951-020-00697-0

23. Uddin MJ, Scoutaris N, Klepetsanis P, *et al.*, 2015, Inkjet printing of transdermal microneedles for the delivery of anticancer agents. *Int J Pharm*, 494(2): 593–602.

    https://doi.org/10.1016/j.ijpharm.2015.01.038

24. Ross S, Scoutaris N, Lamprou D, *et al.*, 2015, Inkjet printing of insulin microneedles for transdermal delivery. *Drug Deliv Transl Res*, 5(4): 451–461.

    https://doi.org/10.1007/s13346-015-0251-1

25. Uddin MJ, Scoutaris N, Economidou SN, *et al.*, 2020, 3D printed microneedles for anticancer therapy of skin tumours. *Mater Sci Eng C Mater Biol Appl*, 107(February): 110248.

    https://doi.org/10.1016/j.msec.2019.110248

26. Tarbox TN, Watts AB, Cui Z, *et al.*, 2018, An update on coating/manufacturing techniques of microneedles. *Drug Deliv Transl Res*, 8(6): 1828–1843.

    https://doi.org/10.1007/s13346-017-0466-4

27. Haj-Ahmad R, Khan H, Arshad MS, *et al.*, 2015, Microneedle coating techniques for transdermal drug delivery. *Pharmaceutics*, 7(4): 486–502.

    https://doi.org/10.3390/pharmaceutics7040486

28. Papazoglou S, Zergioti I, 2017, Laser induced forward transfer (LIFT) of nano-micro patterns for sensor applications. *Microelectron Eng*, 182(October): 25–34.

    https://doi.org/10.1016/j.mee.2017.08.003

29. Kanaki Z, Chandrinou C, Orfanou IM, *et al.*, 2022, Laser-induced forward transfer printing on microneedles for transdermal delivery of gemcitabine. *Int J Bioprint*, 8(2): 554.

    https://doi.org/10.18063/ijb.v8i2.554

30. Hall MD, Telma KA, Chang KE, *et al.*, 2014, Say no to DMSO: dimethylsulfoxide inactivates cisplatin, carboplatin, and other platinum complexes. *Cancer Res*, 74(14): 3913–3922.

    https://doi.org/10.1158/0008-5472.CAN-14-0247

31. Ziesmer J, Tajpara P, Hempel NJ, *et al.*, 2021, Vancomycin-loaded microneedle arrays against methicillin-resistant Staphylococcus aureus skin infections. *Adv Mater Technol*, 6(7): 2001307.

    https://doi.org/10.1002/admt.202001307

32. Shaik AN, Altomare DA, Lesko LJ, *et al.*, 2017, Development and validation of a LC-MS/MS assay for quantification of cisplatin in rat plasma and urine. *J Chromatogr B Analyt Technol Biomed Life Sci*, 1046(March): 243–249.

    https://doi.org/10.1016/j.jchromb.2016.11.027

33. Coughlan AM, Harmon C, Whelan S, *et al.*, 2016, Myeloid engraftment in humanized mice: Impact of granulocyte-colony stimulating factor treatment and transgenic mouse strain. *Stem Cells Dev*, 25(7): 530–541.

    https://doi.org/10.1089/scd.2015.0289

34. Shultz LD, Lyons BL, Burzenski LM, *et al.*, 2005, Human lymphoid and myeloid cell development in NOD/LtSz-scid IL2R gamma null mice engrafted with mobilized human hemopoietic stem cells. *J Immunol*, 174(10): 6477–6489.

    https://doi.org/10.4049/jimmunol.174.10.6477

35. Kanaki Z, Voutsina A, Markou A, *et al.*, 2021, Generation of non-small cell lung cancer patient-derived xenografts to study intratumor heterogeneity. *Cancers (Basel)*, 13(10).

    https://doi.org/10.3390/cancers13102446

36. Falcon-Suarez IH, Livo K, Callow B, *et al.*, 2020, Geophysical early warning of salt precipitation during geological carbon sequestration. *Sci Rep,* 10(1): 16472.

    https://doi.org/10.1038/s41598-020-73091-3

37. Johnsson A, Olsson C, Nygren O, *et al.*, 1995, Pharmacokinetics and tissue distribution of cisplatin in nude mice: Platinum levels and cisplatin-DNA adducts. *Cancer Chemother Pharmacol*, 37(1–2): 23–31.

    https://doi.org/10.1007/BF00685625

38. Rampias T, Karagiannis D, Avgeris M, *et al.*, 2019, The lysine-specific methyltransferase KMT2C/MLL3 regulates DNA repair components in cancer. *EMBO Rep,* 20(3).

    https://doi.org/10.15252/embr.201846821

39. Ray Chaudhuri A, Callen E, Ding X, *et al.*, 2016, Replication fork stability confers chemoresistance in BRCA-deficient cells. *Nature*, 535(7612): 382–387.

    https://doi.org/10.1038/nature18325

40. Chang A, Liu L, Ashby JM, *et al.,* 2021, Recruitment of KMT2C/MLL3 to DNA damage sites mediates DNA damage responses and regulates PARP inhibitor sensitivity in cancer. *Cancer Res*, 81(12): 3358–3373.

    https://doi.org/10.1158/0008-5472.CAN-21-0688

41. Diossy M, Sztupinszki Z, Borcsok J, *et al.*, 2021, A subset of lung cancer cases shows robust signs of homologous recombination deficiency associated genomic mutational signatures. *NPJ Precis Oncol*, 5(1): 55.

https://doi.org/10.1038/s41698-021-00199-8

42. Zhou Z, Ding Z, Yuan J, *et al.*, 2022, Homologous recombination deficiency (HRD) can predict the therapeutic outcomes of immuno-neoadjuvant therapy in NSCLC patients. *J Hematol Oncol*, 15(1): 62.

https://doi.org/10.1186/s13045-022-01283-7

43. Wu S, Zhang Y, Zhang Y, *et al.*, 2022, Mutational landscape of homologous recombination-related genes in small-cell lung cancer. *Cancer Med*, 12(4): 4486–4495.

https://doi.org/10.1002/cam4.5148

44. Chang Q, Ornatsky OI, Koch CJ, *et al.*, 2015, Single-cell measurement of the uptake, intratumoral distribution and cell cycle effects of cisplatin using mass cytometry. *Int J Cancer*, 136(5): 1202–1209.

https://doi.org/10.1002/ijc.29074

45. Skavatsou E, Semitekolou M, Morianos I, *et al.*, 2021, Immunotherapy combined with metronomic dosing: An effective approach for the treatment of NSCLC. *Cancers (Basel)*, 13(8).

https://doi.org/10.3390/cancers13081901

46. Ameri M, Kadkhodayan M, Nguyen J, *et al.*, 2014, Human growth hormone delivery with a microneedle transdermal system: Preclinical formulation, stability, delivery and PK of therapeutically relevant doses. *Pharmaceutics*, 6(2): 220–234.

https://doi.org/10.3390/pharmaceutics6020220

47. Chen X, Prow TW, Crichton ML, *et al.*, 2009, Dry-coated microprojection array patches for targeted delivery of immunotherapeutics to the skin. *J Control Release*, 139(3): 212–220.

https://doi.org/10.1016/j.jconrel.2009.06.029

48. Vrdoljak A, McGrath MG, Carey JB, *et al.*, 2012, Coated microneedle arrays for transcutaneous delivery of live virus vaccines. *J Control Release*, 159(1): 34–42.

https://doi.org/10.1016/j.jconrel.2011.12.026

49. Gill HS, Prausnitz MR, 2007, Coating formulations for microneedles. *Pharm Res*, 24(7): 1369–1380.

https://doi.org/10.1007/s11095-007-9286-4

50. Ingrole RSJ, Gill HS, 2019, Microneedle coating methods: A review with a perspective. *J Pharmacol Exp Ther*, 370(3): 555–569.

https://doi.org/10.1124/jpet.119.258707

51. Bhatnagar S, Kumari P, Pattarabhiran SP, *et al.*, 2018, Zein microneedles for localized delivery of chemotherapeutic agents to treat breast cancer: Drug loading, release behavior, and skin permeation studies. *AAPS PharmSciTech*, 19(4): 1818–1826.

https://doi.org/10.1208/s12249-018-1004-5

52. Infante JR, Benhadji KA, Dy GK, *et al.*, 2015, Phase 1b study of the oral gemcitabine 'Pro-drug' LY2334737 in combination with capecitabine in patients with advanced solid tumors. *Invest New Drugs*, 33(2): 432–439.

https://doi.org/10.1007/s10637-015-0207-9

53. Rose M, Burgess JT, O'Byrne K, *et al.*, 2020, PARP inhibitors: Clinical relevance, mechanisms of action and tumor resistance. *Front Cell Dev Biol*, 8(September): 564601.

https://doi.org/10.3389/fcell.2020.564601

54. Brown TJ, Reiss KA, 2021, PARP inhibitors in pancreatic cancer. *Cancer J*, 27(6): 465–475.

https://doi.org/10.1097/PPO.0000000000000554

55. Beatson EL, Chau CH, Price DK, *et al.*, 2022, PARP inhibitors on the move in prostate cancer: Spotlight on Niraparib & update on PARP inhibitor combination trials. *Am J Clin Exp Urol*, 10(4): 252–257.

56. van der Wiel AMA, Schuitmaker L, Cong Y, *et al.*, 2022, Homologous recombination deficiency scar: Mutations and beyond-implications for precision oncology. *Cancers (Basel)*, 14(17).

https://doi.org/10.3390/cancers14174157

57. Frankenberg-Schwager M, Kirchermeier D, Greif G, *et al.*, 2005, Cisplatin-mediated DNA double-strand breaks in replicating but not in quiescent cells of the yeast Saccharomyces cerevisiae. *Toxicology*, 212(2–3): 175–184.

https://doi.org/10.1016/j.tox.2005.04.015

58. Schierl R, Rohrer B, Hohnloser J, 1995, Long-term platinum excretion in patients treated with cisplatin. *Cancer Chemother Pharmacol*, 36(1): 75–78.

https://doi.org/10.1007/BF00685736